Effects of particle settling on Rayleigh-Bénard convection

Paolo Oresta[1,2] and Andrea Prosperetti[3,4]

[1]*Department of Mathematics, Mechanics and Management, Polytechnic of Bari, 70126 Bari, Italy*

[2]*Department of Engineering for Innovation, University of Salento, and INFN sez. Lecce, 73100 Lecce, Italy*

[3]*Department of Mechanical Engineering, Johns Hopkins University, Baltimore, Maryland 21218, USA*

[4]*Physics of Fluids Group, Department of Science and Technology, J. M. Burgers Centre for Fluid Dynamics, University of Twente, 7500 AE Enschede, The Netherlands*

(Received 14 April 2013; revised manuscript received 6 May 2013; published 20 June 2013)

The effect of particles falling under gravity in a weakly turbulent Rayleigh-Bénard gas flow is studied numerically. The particle Stokes number is varied between 0.01 and 1 and their temperature is held fixed at the temperature of the cold plate, of the hot plate, or the mean between these values. Mechanical, thermal, and combined mechanical and thermal couplings between the particles and the fluid are studied separately. It is shown that the mechanical coupling plays a greater and greater role in the increase of the Nusselt number with increasing particle size. A rather unexpected result is an unusual kind of *reverse one-way coupling*, in the sense that the fluid is found to be strongly influenced by the particles, while the particles themselves appear to be little affected by the fluid, despite the relative smallness of the Stokes numbers. It is shown that this result derives from the very strong constraint on the fluid behavior imposed by the vanishing of the mean fluid vertical velocity over the cross sections of the cell demanded by continuity.

DOI: 10.1103/PhysRevE.87.063014 PACS number(s): 44.25.+f, 47.55.−t, 47.11.−j

I. INTRODUCTION

Buoyancy-induced thermal convection, or Rayleigh-Bénard convection, ranks among the most fundamental fluid dynamic process and, as such, it has been extensively investigated. The vast majority of studies address the single-phase case and several excellent reviews summarize the existing considerable body of knowledge [1–3]. Much less, however, is known for multiphase thermal convection despite its many occurrences, e.g., in the formation of atmospheric precipitation (see, e.g., [4]), magma chambers (see, e.g., [5,6]), boiling (see, e.g., [7]), and counterflow cooling towers (see, e.g., [8]).

In many studies the fluid fills a closed container heated at the bottom and cooled at the top. This situation has been investigated experimentally by Zhong *et al.* [9], who studied the effect of bubble or drop formation in an ethane-filled system, and by Wen and Ding [10], who measured the heat transported by a nanofluid. Schumacher and coworkers [11,12] studied numerically the effect of condensation and evaporation in a gas-vapor mixture focusing on the thermal aspects of phase change but neglecting the mechanical effects of the drops on the flow.

In several earlier papers we have studied numerically the thermal and mechanical effects of bubble formation on the Rayleigh-Bénard problem [13–16]. For this purpose we extended the standard point-bubble model already used for isothermal bubbly flows by several researchers (see, e.g., [17] and [18]) to deal with the thermal effects associated with phase change phenomena.

In the present paper we use a similar approach to model the effect of thermally active particles on the weakly turbulent Rayleigh-Bénard flow of a gas at a Rayleigh number of 2×10^6. We consider a cylindrical system with an aspect ratio (diameter/height) equal to $1/2$ and investigate the effect of the particle size on the flow over a range of Stokes numbers between approximately 0.01 and 1. The particles are assumed to have a large heat capacity so that their temperature does not vary appreciably as they fall through the cell. When the particles maintain the temperature of the cold upper plate, we find a considerable increase in the heat transported, which rapidly increases with the particle size. The effect progressively decreases as the particle temperature increases, the more slowly the larger the particles.

Other researchers have used a similar mathematical model to investigate the effect of particles on turbulent heat transfer in various flows. For example, Shotorban *et al.* [19] studied the temperature statistics in a turbulent shear flow, and both Zonta *et al.* [20] and Arcen *et al.* [21] studied the effect of particles on the heat transfer in a turbulent channel flow. Puragliesi *et al.* [22] studied, by a similar method, Rayleigh-Bénard convection, but their work assumes one-way coupling, with the fluid unaffected by the particles. In our case, the full two-way coupling is considered and is, in fact, one of the main issues of the work, as in order to elucidate the mechanism underlying the effect of the particles, the mechanical, thermal, and combined mechanical-thermal couplings are studied separately.

II. MATHEMATICAL MODEL

We study the problem in the standard Boussinesq approximation augmented by the momentum and energy effects of the particles, treated as points (see Sec. V E for considerations on the validity of this aspect of the model). When the volume occupied by the particles is very small, the fluid continuity equation retains the standard incompressible form,

$$\nabla \cdot \mathbf{u} = 0, \tag{1}$$

in which $\mathbf{u}$ is the fluid velocity field. We write the momentum equation as

$$\rho \frac{D\mathbf{u}}{Dt} = -\nabla p + \mu \nabla^2 \mathbf{u} - \beta \rho (T - T_c)\mathbf{g} + \sum_{i=1}^{N_p} \mathbf{f}_i \delta(\mathbf{x} - \mathbf{x}_i), \tag{2}$$

where D/Dt is the convective derivative; p and T the fluid pressure and temperature fields; ρ, μ, and β the fluid density, dynamic viscosity, and isobaric thermal expansion coefficient, respectively; $\mathbf{g}$ the acceleration of gravity; and T_c the temperature of the cold plate. The summation is over all the N_p particles. In keeping with the point-particle model, $\mathbf{f}_i$ represents the force exerted on the fluid by the point-like particle i located at $\mathbf{x}_i(t)$:

$$\mathbf{f}_i = \frac{\pi}{6} d_p^3 \rho_p \left(\mathbf{g} - \frac{d\mathbf{v}_i}{dt} \right), \tag{3}$$

in which ρ_p is the particle density, d_p is the particle diameter, equal for all particles in each simulation, and $\mathbf{v}_i$ is the particle velocity. Here we have neglected the buoyancy force, which is very small in the case of solid or liquid particles in a gas.

With the neglect of added mass effects and other small contributions, after some rearrangement, the particle equation of motion may be written in the usual form (see, e.g., [23])

$$\frac{d\mathbf{v}}{dt} = \frac{f(\mathrm{Re}_p)}{\tau_p}(\mathbf{u} - \mathbf{v}) + \mathbf{g}, \tag{4}$$

where the fluid velocity is evaluated at the particle position and the viscous relaxation time τ_p is given by

$$\tau_p = \frac{\rho_p d_p^2}{18\mu}. \tag{5}$$

Here and in the following the subscript p refers to particle quantities. The factor

$$f(\mathrm{Re}_p) = 1 + 0.15\mathrm{Re}_p^{0.687}, \tag{6}$$

with $\mathrm{Re}_p = d_p \rho |\mathbf{v} - \mathbf{u}|/\mu$ the particle Reynolds number, accounts for deviations from the Stokes drag law.

The approximations involved in the use of (1) to (6) are standard and are amply discussed in the literature (see, e.g., [24]– [26]). Some comments on the applicability of the point-particle model to the present simulations are given below in Sec. V E.

The model for the fluid energy equation is patterned after that for the momentum equation. We write

$$\rho c \frac{DT}{Dt} = k\nabla^2 T + \sum_{i=1}^{N_p} Q_i \delta(\mathbf{x} - \mathbf{x}_i), \tag{7}$$

where k and c are the fluid thermal conductivity and constant-pressure specific heat and Q_i is the energy source or sink due to the thermal exchange with the ith particle. We model this quantity by means of a heat transfer coefficient $h_{p,i}$, writing

$$Q_i = \pi d_p^2 h_{p,i} [T_{p,i} - T(\mathbf{x}_i)], \tag{8}$$

where $T_{p,i}$ is the temperature of the particle. The heat transfer coefficient is expressed in terms of a single-particle Nusselt number,

$$\mathrm{Nu}_p = \frac{d_p h_p}{k}, \tag{9}$$

for which we use the standard correlation [27],

$$\mathrm{Nu}_p = 2 + 0.6\mathrm{Re}_p^{1/2}\mathrm{Pr}^{1/3}, \tag{10}$$

with $\mathrm{Pr} = \nu/\kappa$ the Prandtl number, given by the ratio of the fluid kinematic viscosity $\nu = \mu/\rho$ to its thermal diffusivity $\kappa = k/\rho c$.

In the present work we assume that the particles maintain the temperature at which they are injected into the fluid. Generally speaking, this approximation is justified in the presence of phase change, or when the residence time of the particles in the flow is short, in view of the comparatively smaller volumetric heat capacity of the fluid; more quantitative considerations on the validity of this approximation are presented in Sec. V E.

It order to better understand the effect of the particles, in addition to simulations based on the complete mathematical model just described, we also describe the results of simulations in which the particles are coupled only mechanically, and not thermally, with the fluid and, conversely, simulations with thermal, but no mechanical, coupling. These "single-effect" simulations are based on Eqs. (2) and (7), in which the terms including summations over Q_i and $\mathbf{f}_i$, respectively, are dropped.

III. CONTROL AND RESPONSE PARAMETERS

The standard single-phase natural convection in the Boussinesq approximation is controlled by the Rayleigh number

$$\mathrm{Ra} = \frac{g\beta(T_h - T_c)H^3}{\nu\kappa}, \tag{11}$$

where $g = |\mathbf{g}|$, T_h and T_c are the temperatures of the hot (bottom) and cold (top) plates, respectively, and H is the height of the cell, by the fluid Prandtl number and by the geometry of the cell, which here is taken to be cylindrical, with radius R and aspect ratio $\Gamma = 2R/H = 1/2$.

We consider as our base case a situation in which, without particles, $\mathrm{Ra} = 2 \times 10^6$ and $\mathrm{Pr} = 0.68$, a value appropriate, for example, for air at 0 °C. With these parameter values, in the absence of particles, the cell contains a single convection roll with fluid rising along one side and descending along the opposite side and a Nusselt number Nu approximately equal to 12. The dimensional values of the parameters used in the simulations are listed in Table I; the particle physical properties are close to those of ice.

We keep the number of particles fixed at $N_p = 25\,000$ and focus on the dependence of the Nusselt number on the particle diameter d_p and, consequently, on the mean particle volume fraction $\langle \alpha_p \rangle = \frac{1}{6}\pi d_p^3 N_p/(\pi R^2 H)$ and on the mass loading $M_p = N_p m_p/(\pi R^2 H \rho)$, with m_p the particle mass given by $m_p = \frac{1}{6}\pi d_p^3 \rho_p$. Other important quantities that depend on the particle diameter are the terminal velocity v_t, given by (4) with $d\mathbf{v}/dt = 0$,

$$v_t = \frac{\tau_p}{f(\mathrm{Re}_t)} g, \tag{12}$$

with $\mathrm{Re}_t = d_p v_t/\nu$, and the characteristic dimensionless residence time

$$\theta = \frac{H/v_t}{H/U_f} = \frac{U_f}{v_t}, \tag{13}$$

in which

$$U_f = \sqrt{g\beta(T_h - T_c)H} \tag{14}$$

TABLE I. Summary of the fluid and particle properties used in the simulations.

Parameter	Value
Aspect ratio, $2R/H$	1/2
Prandtl number, Pr	0.678
Rayleigh number, Ra	2×10^6
Particle number, N_p	25 000
Cell height, H	0.116 m
Cell diameter, $2R$	0.058 m
Temperature difference, $T_h - T_c$	10 °C
Particle density, ρ_p	917 kg/m^3
Fluid density, ρ	1.29 kg/m^3
Kinematic viscosity, ν	1.37×10^{-5} m^2/s
Thermal diffusivity, κ	2.02×10^{-5} m^2/s
Thermal expansion coefficient, β	3.67×10^{-3} K^{-1}
Constant-pressure fluid specific heat, c	1 000 J/kg
Free-fall velocity, U_f	2.04×10^{-1} m/s

is the free-fall velocity. Nondimensional times are consistently expressed in terms of H/U_f.

Two Stokes numbers can be defined, one based on the fluid free-fall velocity

$$\mathrm{St}_f = \frac{\tau_p U_f}{H} \tag{15}$$

and one based on the Kolmogorov time scale $\sqrt{\nu/\epsilon}$,

$$\mathrm{St}_K = \tau_p \sqrt{\frac{\epsilon}{\nu}}, \tag{16}$$

with ϵ the energy dissipation rate. The latter quantity can be estimated from the well-known exact relation valid for single-phase Rayleigh-Bénard convection (see, e.g., Ref. [2])

$$\epsilon = \frac{\nu^3}{H^4} \frac{\mathrm{Ra}}{\mathrm{Pr}^2} (\mathrm{Nu} - 1). \tag{17}$$

With the present parameter values, for single-phase convection, we find approximately $\sqrt{\nu/\epsilon} \simeq 0.157$ s. Dimensional numerical values for various particle quantities of interest are listed in Table II, and nondimensional ones in Table III.

We consider three particle temperatures, "cold" particles, with $T_p = T_c$, "hot" particles, for which $T_p = T_h$, and "warm"

TABLE II. Mean volume fraction $\langle \alpha_p \rangle_{V,t}$, particle terminal velocity v_t, residence time scale H/v_t, characteristic particle time scale τ_p, and particle mass m_p corresponding to the particle diameters used in the simulations.

d_p (μm)	$10^5 \langle \alpha_p \rangle_{V,t}$	v_t (mm/s)	H/v_t (s)	τ_p (ms)	m_p (ng)
25	0.067	17.4	6.62	1.80	7.50
50	0.534	66.6	1.72	7.14	60.0
75	1.80	141	0.815	16.2	202
100	4.27	232	0.495	28.8	480
125	8.34	334	0.344	44.9	937
150	14.4	438	0.262	64.7	1620
175	22.9	550	0.209	88.1	2572
200	34.2	658	0.175	115	3839

TABLE III. Dimensionless particle parameters as functions of the particle diameter d_p: mass loading $M_p = \frac{\pi}{6} d_p^3 \rho_p N_p / (\pi R^2 H \rho)$; dimensionless terminal velocity (or inverse dimensionless residence time in the cell) v_t/U_f; Reynolds and Péclet numbers based on the terminal velocity, Re_t and Pe_t; Kolmogorov-scale Stokes number St_K; and large-scale Stokes number St_f.

d_p (μm)	$10^2 M_p$	v_t/U_f	$10^2 v_t \tau_p / H$	Re_t	Pe_t	$10^3 \mathrm{St}_K$	$10^3 \mathrm{St}_f$
25	0.049	0.0852	0.027	0.0318	0.0216	12.6	3.17
50	0.395	0.327	0.415	0.244	0.165	50.4	12.7
75	1.33	0.692	1.98	0.775	0.525	113	28.6
100	3.16	1.14	5.79	1.70	1.15	201	50.8
125	6.17	1.64	13.0	3.06	2.07	315	79.4
150	10.7	2.15	24.5	4.81	3.26	452	114
175	16.9	2.70	42.1	7.05	4.78	619	156
200	25.3	3.23	65.6	9.64	6.54	805	203

particles, with $T_p = T_m$, where

$$T_m \equiv \tfrac{1}{2}(T_h + T_c), \tag{18}$$

is the mean of the hot- and cold-plate temperatures.

The parameter space of the problem is large and it is not possible to explore it fully in a project of reasonable scope. While the situation we have chosen is rather far from what might be considered as fully developed turbulent Rayleigh-Bénard convection, this choice permits us to explore in detail the effect of the particle size and temperature, which are parameters of primary importance in the problem.

In steady single-phase natural convection the heat flux into the base of the cell (located at $z = 0$) equals that out of the top (located at $z = H$). The corresponding Nusselt numbers Nu_h and Nu_c at the hot and cold plates are equal and can be calculated from

$$\mathrm{Nu}_h = \mathrm{Nu}_c = -\frac{H}{T_h - T_c} \langle \partial_z T \rangle_{A,t}|_{z=0,H}. \tag{19}$$

Here ∂_z denotes the derivative in the upward vertical direction and $\langle (\cdots) \rangle$ indicates mean values with the average taken over the subscripted quantities, i.e., here, the cross-sectional area A and the time t. The same convention is followed consistently in this paper to indicate averages of fluid quantities.

In the presence of particles the equality between Nu_h and Nu_c no longer holds, as part of the energy is taken up or released by the particles. By integration of the energy equation over the cell volume it was shown in Ref. [13] that

$$\mathrm{Nu}_h = 1 + \frac{H}{\kappa (T_h - T_c)} \langle u_z (T - T_c) \rangle_{V,t} - \frac{1}{\pi R^2 k (T_h - T_c)} \left\langle \sum_i (H - z_i) Q_i \right\rangle_t \tag{20}$$

and

$$\mathrm{Nu}_c = 1 + \frac{H}{\kappa (T_h - T_c)} \langle u_z (T - T_c) \rangle_{V,t} + \frac{1}{\pi R^2 k (T_h - T_c)} \left\langle \sum_i z_i Q_i \right\rangle_t. \tag{21}$$

In the case of single-phase flow, $Q_i = 0$ and these two expressions become equal, as expected, and give an alternative, although equivalent, form for the single-phase Nusselt number, namely,

$$\mathrm{Nu}_h = \mathrm{Nu}_c = 1 + \frac{H}{\kappa(T_h - T_c)}\langle u_z(T - T_c)\rangle_{V,t}.$$

The first term on the right-hand sides of (20) and (21) is due to conduction, the second one to convection, and the last one is the particle contribution.

In order to understand the effect of the particles on the convection in the cell it is also useful to consider the azimuthal Fourier modes E_n of the fluid kinetic energy distribution. These quantities are defined by

$$E_n = \frac{\pi}{\beta g H^4 (T_h - T_c)} \int_0^R r dr \int_0^H dz \langle |\mathbf{u}_n|^2 \rangle_t, \qquad (22)$$

in which $\mathbf{u}_n$ is the nth Fourier coefficient of the vector velocity field in the angular variable. The mode $n = 0$ corresponds to a toroidal circulation symmetric around the vertical axis of the cylinder, while the mode $n = 1$ has the form of a vortex around a horizontal axis. In the particle-free case it is found that the circulation transitions from a dominant $n = 0$ state to an $n = 1$ state as the Rayleigh number is increased. In this sense, we can think of the $n = 0$ mode as a lower energy mode compared with the $n = 1$ mode.

IV. NUMERICAL METHOD AND PROCEDURE

The numerical method used in this work has been described in our previous publications (see especially [13]) and only the essential aspects are summarized here. We solve the continuity, momentum, and energy equations in a cylindrical domain of radius R and height H. No-slip conditions are applied on all the solid surfaces. The temperature of the top and bottom surfaces is kept constant at T_c and T_h, respectively, while the lateral boundary is assumed to be adiabatic.

The Navier-Stokes equations are solved in a cylindrical coordinate system using a second-order, finite difference, fractional-step method on a staggered grid. The advective terms are treated explicitly, the viscous terms implicitly, and the Runge-Kutta third order scheme is used for time marching.

According to the Kolmogorov theory (see, e.g., [2]), the size of the dissipative length scales η can be estimated as $\eta/H = \mathrm{Re}^{-3/4}$, where Re is the Reynolds number based on the cell height and the root-mean-square fluid velocity. With a maximum Re of order 800, we find $\eta/H \simeq 6.6 \times 10^{-3}$, which is adequately resolved by our grid of $193 \times 49 \times 193$ nodes in the azimuthal, radial, and axial directions, respectively, as shown in our previous work [13,16]. We have used the same number of nodes for all the simulations described in this paper, clustering them near the top and bottom plates and the side wall. As a result of this clustering, at least 10 nodes fall in the viscous boundary layers on the side walls (estimated as the cell radius divided by the square root of the largest value of the Reynolds number encountered in the present simulations) and at least 15 in the thermal layers adjacent to the plates (estimated as the cell height divided by the largest value of the Nusselt number, since the strongest circulation takes place with cold particles, which bring the temperature at the edge of the hot boundary layer close to T_c rather than T_m as in ordinary Boussinesq single-phase convection; see Fig. 5).

Once the flow fields of the fluid phase have been calculated, the new particle velocity is found by an implicit integration of the particle momentum equation, (4), by the trapezoidal rule; the particle position is updated by the third-order Runge-Kutta method.

The (dimensionless) time step Δt is smaller than the lesser between the Stokes number St_K and the time required for a particle to cross a computational cell. For mechanically coupled 200-μm particles we have run tests halving Δt from 10^{-3} to 0.5×10^{-3}, finding differences of less than 1%.

Upon integration of the fluid momentum and energy equations over a computational cell, the contribution of the particles is localized at their position and this effect must be replaced by an equivalent one localized at the computational nodes. This objective is achieved by a second-order-accurate interpolation as described in Ref. [13]. The interpolation preserves the resultant and the couple of the particle forces, as well as the total amount of heat that each particle exchanges with the fluid.

When a particle reaches the bottom of the cell, it is removed from the calculation and a new particle is reinjected at a random position on the top plate. If this particle is given a velocity equal to that of the surrounding fluid (which, near the plate, is very low), it takes some time to accelerate. As a consequence, a particle-rich layer forms near the top plate the thickness of which increases as the settling velocity decreases. This feature is demonstrated in Fig. 1, which shows the time- and area-averaged particle number density $\langle n \rangle_{A,t}$ normalized by the volumetric number density, $n_0 = N_p/(\pi R^2 H)$, for $d_p =$ 25, 100, 175, and 200 μm. This particle accumulation would obscure the comparison among the effects of different particle radii. To avoid this shortcoming, we reinject the particles with a downward velocity equal to the settling velocity. In practice, this may model a liquid spray falling through the gas. As shown later after (26), the mean fraction of particles N_{inj}/N_p reinjected per unit dimensionless time is about v_t/U_f.

At injection, the particle temperature is set to T_c, T_h, or $T_m = \frac{1}{2}(T_h + T_c)$ as noted before. We found that the "hot" particles with $T_p = T_h$ result in a nearly complete suppression

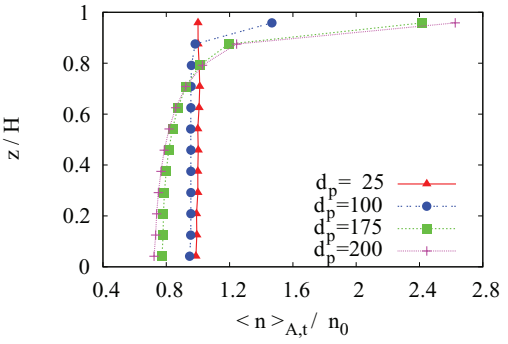

FIG. 1. (Color online) Area- and time-averaged normalized number density of thermally and mechanically coupled "cold" particles as a function of height in the cell; $d_p = 25$ μm [(red) triangles], $d_p = 100$ μm [blue (circles)], $d_p = 175$ μm [(green) squares], and $d_p = 200$ μm [(purple) crosses]. These are the only simulations described in this paper in which particles are injected at the top plate with the local fluid velocity.

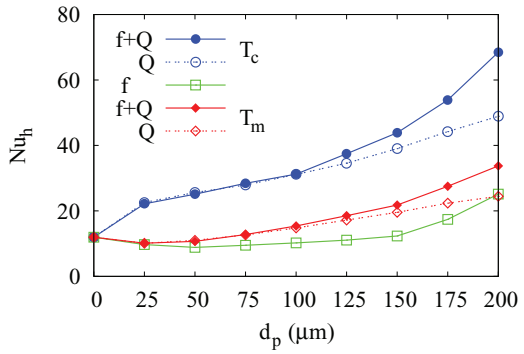

FIG. 2. (Color online) Hot-plate Nusselt number as a function of the particle diameter d_p for "cold" [circles and (blue) lines] and "warm" [diamonds and (red) lines] particles ($T_p = T_c$ and $T_p = T_m$, respectively). Dashed lines (open symbols; labeled Q) show results with thermal coupling only; solid lines (filled symbols; labeled $f + Q$), with combined thermal and mechanical coupling. The bottommost (green) line (open squares; labeled f) shows results for mechanical coupling only, which are independent of the particle temperature.

of convection in the cell. Accordingly, we show only very limited results for this case.

V. RESULTS

Figure 2 summarizes the results of the present study in the form of a graph showing the dependence of the bottom-plate Nusselt number, Nu_h, vs the particle diameter with mechanical, thermal, or combined mechanical and thermal couplings. Circles with (blue) lines represent the case of "cold" particles, i.e., with $T_p = T_c$, and diamonds with (red) lines, "warm" particles, i.e., with $T_p = \frac{1}{2}(T_h + T_c)$. Here and in the following, filled symbols denote results with combined thermal and mechanical fluid-particle coupling, while open symbols refer to either thermal or mechanical coupling only. The case with hot particles, i.e., $T_p = T_h$, is dealt with briefly later.

These results become clearer if we consider at the same time the Reynolds number Re of the fluid flow, which is shown in Fig. 3 with the same symbols and line types as in Fig. 2. This quantity is calculated on the basis of the cell height and of the

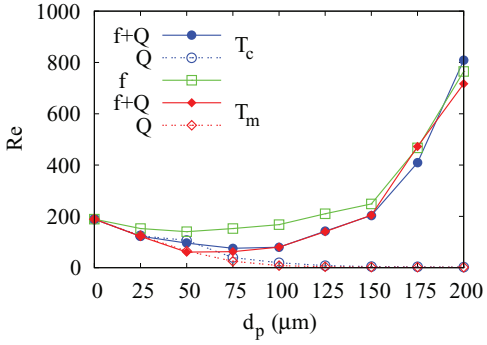

FIG. 3. (Color online) Fluid Reynolds number (based on the volume- and time-averaged r.m.s. velocity) as a function of particle diameter d_p for "cold" [circles and (blue) lines] and "warm" [diamonds and (red) lines] particles ($T_p = T_c$ and $T_p = T_m$, respectively). See the caption to Fig. 2 for further details.

r.m.s. velocity $\sqrt{\langle u^2 \rangle_{V,t}}$, which provides a good estimate of the mean velocity in the cell.

A. Mechanical coupling

In order to understand the results in Figs. 2 and 3 it is useful to start by neglecting the fluid-particle heat exchange, focusing only on the mechanical coupling shown, here and in the subsequent figures, by squares [and (green) lines]. It is shown that, as the particle diameter increases, both the Nusselt and the Reynolds numbers initially decrease and then increase. The decrease is due to the drag that the particles exert on the fluid, especially in the cold and hot boundary layers near the top and bottom plates, where their velocity tends to be approximately perpendicular to that of fluid. In principle, this effect could be counteracted by an accumulation of lighter particles in the descending stream, which would increase its velocity, as one might expect on the basis of the behavior of bubbles in Rayleigh-Bénard convection, which are swept up and accumulate in the ascending stream [16]. However, with the present parameter values, this phenomenon does not occur even for 25-μm particles, as we have found by calculating the position of the center of mass of the particle distribution over the cross sections throughout the cell height. For all particle diameters, we have consistently found that the center of the particle distribution coincides with the axis of the cell to within less than $10^{-3}H$. Thus the particles can be considered to be uniformly distributed over the horizontal cross section so that the acceleration that they impart to the colder, descending fluid stream is balanced by the retardation that they cause on the warmer, ascending stream. What remains is the drag they impose on the flow in the thermal boundary layers, which is responsible for the decline of both Nu_h and Re caused by the smaller particles shown in Figs. 2 and 3.

The marked increase in the Reynolds number with particle size after the minimum at around $d_p \simeq 50$ μm is due to the gradual prevailing of an opposing mechanism. As the particles fall, they drag fluid with them, and the effect increases with the particle diameter (see also Fig. 10). The consequences of this effect are evident in Fig. 4, which shows instantaneous snapshots of the vertical velocity on the cross section at the midplane of the cell, $z = \frac{1}{2}H$, for the single-phase case and for $d_p = 25$, 100, and 200 μm. It can be seen there that, as the particle size increases, the fraction of area occupied by descending fluid increases. Since, by continuity, the mean fluid vertical velocity on each cross section must vanish, the narrowing of the ascending stream causes the ascending fluid to increase its speed and both the heat flux and Re increase. [A careful analysis of the numerical results shows that the very slight anomaly visible near the center of Fig. 4(d) is a plotting artifact, and not the manifestation of an insufficiently accurate treatment of the singularity on the axis of the cell.]

These conclusions are corroborated by Figs. 5 and 6, which show, respectively, the time- and volume-averaged temperature in the cell and the contribution of the convective term to the Nusselt number, both as functions of the particle diameter d_p. It is well known that, in the Boussinesq approximation, in the single-phase case the mean temperature in the cell is very close to $T_m = \frac{1}{2}(T_h + T_c)$ (see, e.g., [2]). Again focusing on the results for purely mechanical coupling [squares with (green)

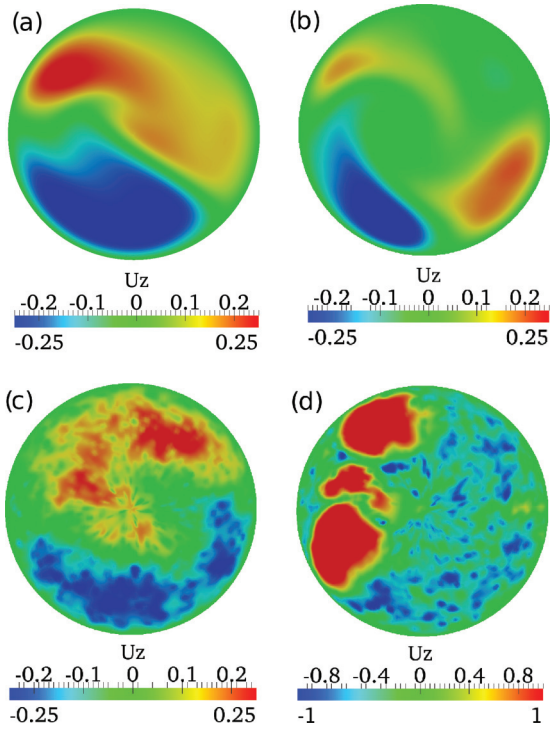

FIG. 4. (Color online) Vertical fluid velocity on the midplane cross section at $z = \frac{1}{2}H$ for purely mechanical coupling: (a) single phase, (b) $d_p = 25$ μm, and (c) $d_p = 100$ μm, (*d*) $d_p = 200$ μm; note the enlarged scale for the latter case.

lines], we see that the temperature is close to this value for the smaller particles but then decreases slightly with d_p as the descent of the colder fluid is aided by the falling particles. The convective contribution to the Nusselt number [second term in Eq. (20)] follows a trend similar to that in Fig. 3 for the Reynolds number.

Further insight into the nature of the flow in the cell can be gained by considering the distribution of the mean fluid kinetic energy among the different azimuthal Fourier modes defined in Eq. (22). Figure 7 shows the ratio E_1/E_0 vs the particle diameter. Without particles this ratio is close to 3, indicating a flow structure dominated by an annular mode with an approximately horizontal axis as explained after (22). As

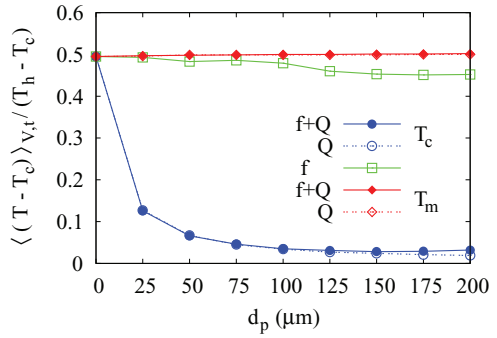

FIG. 5. (Color online) Volume- and time-averaged fluid temperature as a function of the particle diameter d_p for "cold" [circles and (blue) lines] and "warm" [diamonds and (red) lines] particles ($T_p = T_c$ and $T_p = T_m$, respectively). See the caption to Fig. 2 for further details.

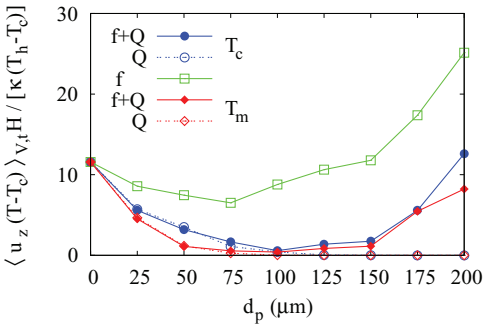

FIG. 6. (Color online) Volume-averaged convective contribution to the hot-plate Nusselt number, Eq. (20), as a function of the particle diameter d_p for "cold" [circles and (blue) lines] and "warm" [diamonds and (red) lines] particles ($T_p = T_c$ and $T_p = T_m$, respectively). See the caption to Fig. 2 for further details.

the particle diameter increases, this mode is weakened and the nearly axisymmetric toroidal vortex structure becomes more prominent, until the annular mode returns to dominate for large particles. These features can be recognized in the sample fluid particle trajectories shown in the three-dimensional views in Fig. 8; the vertical velocity distributions in the cross sections located at $z/H = 0.05$, 0.5, and 0.95 are also shown there.

The lines in Fig. 7 show local maxima for several values of the particle diameter in the different cases, but not too much can be read in these features, as modes 0 and 1 are insufficient to fully characterize the flow in the cell. Indeed, while the energy of some higher modes, especially modes 2 and 3, is lower, it is comparable to that of modes 0 and 1. These local features (which we confirmed by averaging over significantly longer simulations in several cases) are due to subtle redistributions of the energy among the various modes. For example, the maximum at $d_p = 75$ μm in the mechanical coupling case [squares with (green) line] is found to correspond to a slight decrease in E_2 and E_3, to the benefit of E_1.

B. Thermal coupling

Let us now turn to the converse case, in which mechanical coupling is absent and only the thermal interaction between fluid and particles is considered (dashed linesand open symbols

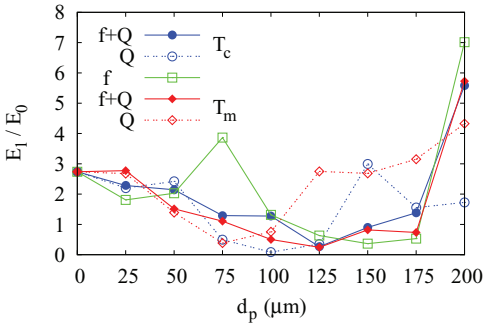

FIG. 7. (Color online) Ratio E_1/E_0 of the first two angular Fourier modes of the kinetic energy defined in Eq. (22) as a function of the particle diameter d_p for "cold" [circles and (blue) lines] and "warm" [diamonds and (red) lines] particles ($T_p = T_c$ and $T_p = T_m$, respectively). See the caption to Fig. 2 for further details.

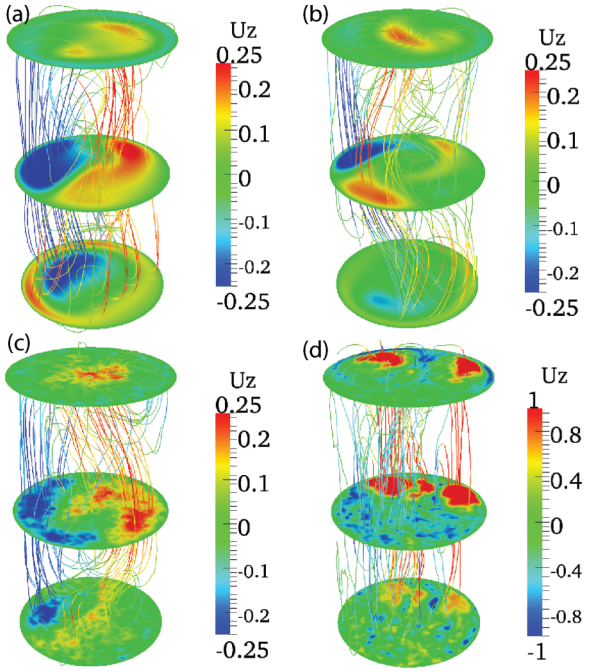

FIG. 8. (Color online) Trajectories of randomly selected fluid particles, with the color keyed to the local vertical velocity for purely mechanical coupling. Instantaneous vertical velocities on the cross sections at $0.05H$, $0.5H$, and $0.95H$ are shown similarly to Fig. 4: (a) single phase, (b) $d_p = 25$ μm, (c) $d_p = 100$ μm, and (d) $d_p = 200$ μm; note the enlarged scale for the last case.

in Figs. 2 and 3 and 5–7). The important physical process to keep in mind is embodied in the last term of (20):

$$-\frac{1}{\pi R^2 k(T_h - T_c)}\left\langle \sum_i (H - z_i) Q_i \right\rangle_t$$

$$= \frac{d_p^2}{R^2 k(T_h - T_c)}\left\langle \sum_i (H - z_i) h_{p,i}[T_i - T_p] \right\rangle_t . \quad (23)$$

For cold particles [$T_p = T_c$; circles and (blue) lines], the local fluid temperature T_i is mostly higher than the particle temperature T_p, the fluid loses heat, and this term gives a positive contribution to the Nusselt number (Fig. 2) the larger $H - z_i$, i.e.,, the closer the particle is to the hot base of the cell. It is evident that cooling the fluid in this region will increase the heat subtracted from the hot plate, and all the more as the heat is subtracted closer to it. This is the origin of the strong increase in the Nusselt number with d_p visible in Fig. 2. For particles smaller than about 125 μm this effect is actually dominant with respect to the mechanical forcing, the addition of which gives nearly indistinguishable results (filled symbols and solid line). For warm particles [$T_p = T_m$; diamonds and (red) lines and diamonds], the effect portrayed by (23) is much weaker as the local fluid temperature over most of the fluid volume is very close to T_m, as also shown in Fig. 5. The cause of the increase in Nu_h as d_p exceeds about 50 μm in this case is due to the fact that the fluid-particle temperature difference in Eq. (23) is weighted by $H - z_i$: the cooling of the fluid where $T_i < T_m = T_p$ occurs near the upper cold surface, where $H - z_i$ is small, while heating occurs near the hot base, where $H - z_i$ is larger. For both cold and warm particles the increase with d_p is approximately linear as $d_p^2 h_p = k d_p \mathrm{Nu}_p$ and the dependence of Nu_p on d_p is fairly weak.

With thermal coupling only, the Reynolds number quickly becomes unimportant (Fig. 3) as the particles tend to render the fluid temperature approximately uniform over the cell, thus weakening the very cause of the circulatory flow. For the same reason, the convective contribution to the Nusselt number becomes less and less important with d_p (Fig. 6) as, with an approximately uniform T, $\langle u_z(T - T_c)\rangle_{V,t} \simeq \langle T - T_c\rangle_{V,t}\langle u_z\rangle_{V,t} = 0$. This strong effect of the thermal coupling on the fluid temperature is demonstrated by the near-equality of the mean fluid temperature with or without the addition of mechanical coupling (Fig. 5).

C. Mechanical and thermal coupling

It is now easier to understand the results for the combined thermal and mechanical couplings. Figure 2 shows that, in the case of cold particles, Nu_h is always greater than for the single-phase case. Up to $d_p \simeq 125$ μm this is the result of the thermal coupling only. For larger particles the increased circulation described before proves beneficial and gives a further strengthening of the heat subtracted from the hot plate. At the same time, the convective contribution to Nu_h strengthens considerably (Fig. 6). The increased circulation also proves beneficial for warm particles, although to a lesser extent. In both cases the Reynolds number is found to be little affected by the thermal coupling due to the mechanical strengthening of the circulation.

D. Further aspects

The previous considerations can be complemented by analyzing several other aspects of the phenomena of present interest with combined thermal and mechanical coupling.

Figure 9 shows the area-averaged particle vertical velocity as a function of height for particles with diameters of 25 μm [triangles with (red) line], 100 μm [circles with (blue) line], 175 μm [squares with (green) line], and 200 μm [crosses with (purple) line]. The vertical component of the particle momentum equation, (4), averaged over time and all the

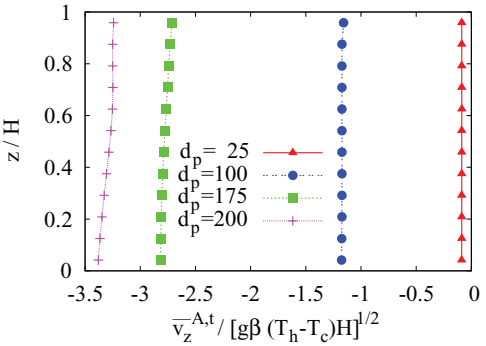

FIG. 9. (Color online) Average vertical velocity of thermally and mechanically coupled "cold" particles as a function of height in the cell for $d_p = 25$ μm [(red) triangles], $d_p = 100$ μm [(blue) circles], $d_p = 175$ μm [(green) squares], and $d_p = 200$ μm [(purple) crosses].

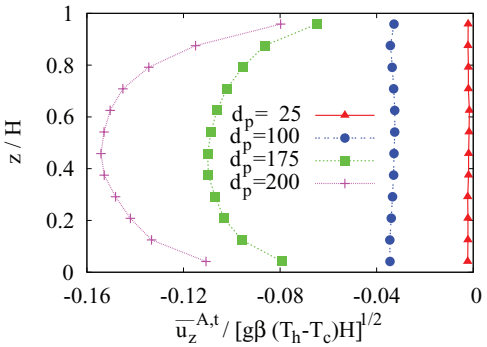

FIG. 10. (Color online) Average fluid vertical velocity at the particle position as a function of height in the cell for thermally and mechanically coupled "cold" particles: $d_p = 25\ \mu$m [(red) triangles], $d_p = 100\ \mu$m [(blue) circles], $d_p = 175\ \mu$m [(green) squares], and $d_p = 200\ \mu$m [(purple) crosses].

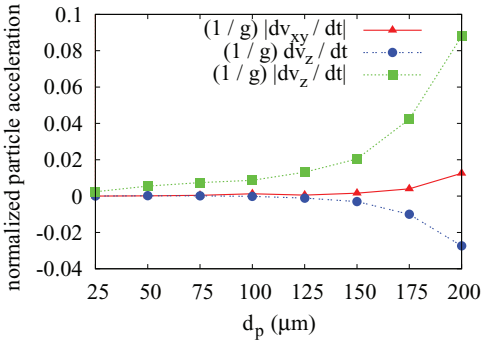

FIG. 11. (Color online) Vertical [(blue) circles] and horizontal [(red) triangles] mean accelerations of thermally and mechanically coupled "cold" particles as functions of the particle diameter d_p. The (green) squares and line show the mean of the modulus of the vertical acceleration. All accelerations are normalized by division by g.

particles in a cross section (indicated by an overline with superscripts A,t) may be written as

$$\overline{v_z}^{A,t} = \overline{u_z}^{A,t} - v_t \overline{\frac{f(\mathrm{Re}_t)}{f(\mathrm{Re}_p)}\left(1 + \frac{1}{g}\frac{dv_z}{dt}\right)}^{A,t}, \qquad (24)$$

in which v_t is the terminal velocity defined in Eq. (12). If the particles sampled all points of the cross section equally and had a small effect on the fluid velocity, we would have $\overline{u_z}^{A,t} = \langle u_z \rangle_{A,t} = 0$. For small particles inertia is unimportant and $f(\mathrm{Re}_t) \simeq f(\mathrm{Re}_p) = 1$ so that one expects that $\overline{v_z}^{A,t} = -v_t$, which is indeed the result shown in Fig. 9 for $d_p = 25\ \mu$m.

The results for larger particles deviate more and more from this prediction. The origin of this feature can be seen in Fig. 10, which shows $\overline{u_z}^{A,t}$, namely, the mean of the fluid velocity at the particle position. As the figure shows, this mean value becomes more and more negative as the particle size increases and contributes to the particle downward velocity as (24) shows. This result might seem unexpected since, as mentioned before, our particles are very nearly uniformly distributed over the cross section, and the mean fluid velocity over any cross section must vanish. By averaging over a considerably longer time we have satisfied ourselves that this result is not an artifact of an insufficient sampling of the cross section. Rather, its origin must be sought in the fact that larger particles drag down the surrounding fluid with them. The effect is a marked reduction in the cross section occupied by the ascending fluid, an increase in its upward velocity, and a consequent increase in the convective transport as mentioned before.

As shown in Eq. (24), two other factors contribute to a difference between the mean settling velocity $\overline{v_z}^{A,t}$ and the terminal velocity v_t. The first one is the particle acceleration, the importance of which can be estimated from Fig. 11, which shows the volume- and time-averaged normalized particle accelerations:

$$\frac{1}{g}\overline{\left|\frac{dv_z}{dt}\right|}^{V,t}, \quad \frac{1}{g}\overline{\frac{dv_z}{dt}}^{V,t}, \quad \frac{1}{g}\overline{\left|\frac{dv_h}{dt}\right|}^{V,t}, \qquad (25)$$

with v_h the horizontal velocity. For $d_p < 100\ \mu$m all acceleration components are virtually 0. Inertia becomes more important for larger particles, although the accelerations are still only a few percent of gravity at the most. Interestingly, the mean of dv_z/dt is negative, which implies a mean downward acceleration, and is smaller in modulus than the mean of $|dv_z/dt|$ so that there are regions where the acceleration is upward.

Conservation of the particle number under steady-state conditions dictates that the area- and time-averaged vertical particle flux $\langle n v_z \rangle_{A,t}$ be independent of z. We have verified that constancy of the vertical particle flux holds to better than 0.5% in all our simulations. Since, as shown in Fig. 9, the particle velocity increases slightly with height (particularly for the larger particles), we then expect the particle concentration to decrease, as indeed is found in Fig. 12 (although, of course, $\langle n v_z \rangle_{A,t}$ is not precisely equal to the product $\langle n \rangle_{A,t} \langle v_z \rangle_{A,t}$).

Introducing the particles at their terminal velocity has the consequence that $\langle n v_z \rangle_{A,t}|_H = \langle n \rangle_{A,t}|_H v_t$, where $\langle n \rangle_{A,t}|_H$ is the mean number density at the upper plate. Figure 13 shows the normalized flux

$$F_z^* = \frac{\langle n v_z \rangle_{A,t}|_{z=0}}{n_0 v_t}, \qquad (26)$$

as a function of the particle diameter. This quantity is essentially 1, rising to just short of 1.03 for $d_p = 200\ \mu$m.

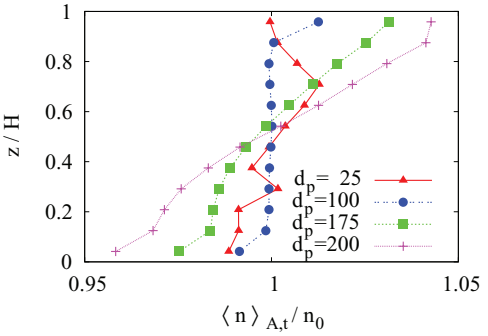

FIG. 12. (Color online) Area- and time-averaged normalized number density of thermally and mechanically coupled "cold" particles as a function of height in the cell: $d_p = 25\ \mu$m [(red) triangles], $d_p = 100\ \mu$m [(blue) circles], $d_p = 175\ \mu$m [(green) squares], and $d_p = 200\ \mu$m [(purple) crosses].

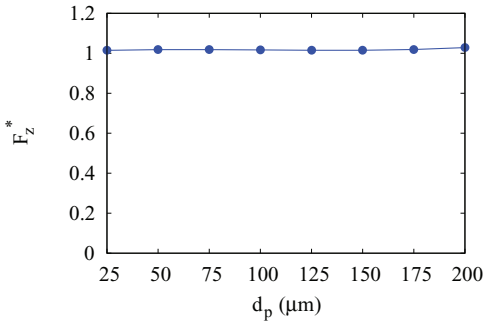

FIG. 13. (Color online) Normalized particle flux, defined in Eq. (26), at the bottom plate as a function of the particle diameter for mechanically and thermally coupled cold particles, $T_p = T_c$.

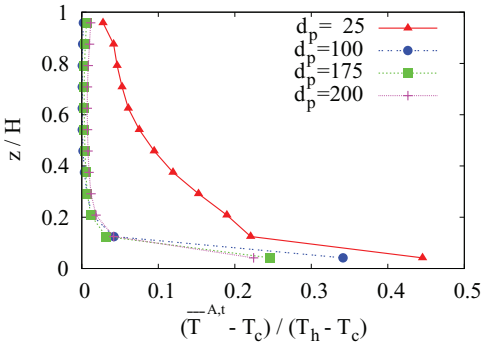

FIG. 14. (Color online) Area- and time-averaged normalized fluid temperature at the particle location for thermally and mechanically coupled "cold" particles as a function of height in the cell: $d_p = 25\ \mu$m [(red) triangles], $d_p = 100\ \mu$m [(blue) circles], $d_p = 175\ \mu$m [(green) squares], and $d_p = 200\ \mu$m [(purple) crosses].

These data are for cold particles with full mechanical and thermal coupling, but results with either coupling and different temperatures are basically indistinguishable. If the particles maintained a uniform number density equal to n_0, the volume average, and fell undisturbed at their terminal velocity, we would have $\langle n v_z \rangle_{A,t} = n_0 v_t$ and $F_z^* = 1$. The closeness of the computed F_z^* to 1 is a further indication of the apparent decoupling of the particles from the fluid discussed in Sec. V E.

We can use this result for a further consistency check on the calculation as the number of particles introduced per unit time at the top of the cell must be given by the product of the cross-sectional area times $\langle n v_z \rangle_{A,t}$. The result of this calculation matches the direct counting of particles introduced per unit time. Figure 13 shows that this number is very close to $\pi R^2 n_0 v_t = N_p v_t / H$ or, in dimensionless form, $N_p v_t / U_f$.

E. Discussion

The results shown and, in particular, those in Fig. 13 for F_z^*, suggest a very unusual sort of "one-way coupling" between the fluid and the particles, which is exactly the opposite of what this denomination usually implies. Indeed, we have found that the particles seem to be little influenced by the flow of the fluid, while they have a very strong effect on it. This conclusion is unexpected and appears inconsistent with the smallness of both large-scale and Kolmogorov-scale Stokes numbers listed in Table III. The resolution of the paradox lies in the very strong constraint that the vanishing of the area-averaged fluid vertical velocity imposes on the system. As noted in connection with expression (24) for the mean particle velocity, particles so small as to be nearly passive tracers might well follow the fluid's fluctuating velocity, but nevertheless, on average, they must fall at their terminal velocity. Very heavy particles would not follow the fluid but would also essentially fall at their terminal velocity. Thus $\overline{v_z}^{A,t}$ must equal v_t for both small and large particles so that its behavior in between these limits is severely constrained. The situation would be different for particles or bubbles in a liquid, where the acceleration term in Eq. (24) might be expected to play a much stronger role.

Two major aspects of the particle model used in this work are worth discussing: the point-like approximation and the assumption of a constant temperature. The former is justified provided the particles are smaller than the smallest fluid scale. With the estimate of the Kolmogorov scale given in Sec. IV, we find that the smallest value of η in our simulations is nearly a factor of 4 larger than the largest particles. This circumstance justifies the applicability of the point-particle model to these particles and, *a fortiori*, to the smaller ones. In any event, a careful examination of this aspect of the present work must await further improvement of the current state of the art.

As for the assumption of a constant particle temperature we may note that, at a qualitative level, it may be expected that allowing cold particles to heat up would give results intermediate between those found for cold and those for warm particles, and similarly for heated-up warm particles. At a more quantitative level, one may compare the duration of the particles' exposure to the fluid with the time scale for a change in their temperature, namely, $c_p m_p / (\pi d_p^2 h_p)$, with c_p the particle specific heat (close to 2050 J/kg for ice at the melting point). For this analysis to be meaningful, it must be based on the effective particle-fluid temperature difference, rather than on the temperature difference $T_h - T_c$ between the hot and the cold plates. Figure 14 shows the mean fluid temperature at the particle position as a function of height in the cell for mechanically and thermally coupled cold particles with diameters of 25, 100, 175 and 200 μm. Aside from the smallest particles, a significant temperature difference only exists near the bottom plate over a thickness of a few percent of the cell height. If we estimate the exposure time as 4% of the cell height divided by the terminal velocity, the ratio of the two time scales ranges from about 20 for $d_p = 25\ \mu$m to 0.01 for $d_p = 200\ \mu$m, with an approximately inverse proportionality to d_p^4. The temperature change may therefore be expected to be negligible for particles larger than about 50 μm, but not necessarily so for smaller particles. For ice particles, heating up will be preceded by melting. The dimensionless ratio relevant here is the energy that a particle receives during its exposure to the warmest fluid, namely, $\pi d_p^2 h_p (T_h - T_c)$, multiplied by the exposure time, to the energy necessary to melt it, $m_p h_{fg}$ (with h_{fg} the latent heat of fusion, approximately 334 kJ/kg for ice). With the maximum temperature difference lasting the time to fall through 4% of the cell height, this ratio, which is also approximately inversely proportional to d_p^4, varies

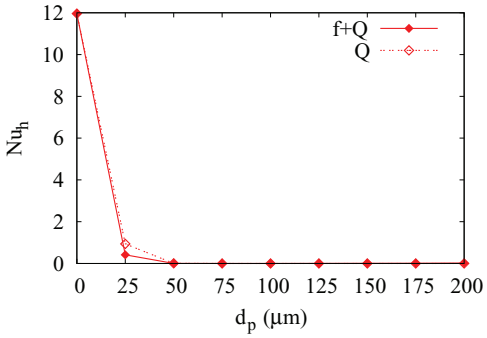

FIG. 15. (Color online) Hot-plate Nusselt number as a function of the particle diameter d_p for "hot" particles, $T_p = T_h$. The dashed line (labeled Q) shows results with thermal coupling only, and the solid line (labeled $f + Q$) results with combined thermal and mechanical coupling.

between about 6 and 0.003. Thus, again, smaller particles may be expected to melt and heat up. The situation is similar for warm particles, whose exposure to a temperature very different from their own is also limited as suggested by Fig. 5. The precise consequences of the thermal response of small particles therefore remains an interesting point, which we plan to address in future studies.

F. "Hot" particles

As the temperature of the settling particles increases, the mean temperature difference between the lower and the upper parts of the cell decreases and the buoyant convection becomes weaker and weaker. In the case of hot particles, with $T_p = T_h$, the effect is to essentially completely stop the convection except for the smallest particles. This is demonstrated in Fig. 15, which shows the Nusselt number at the hot plate as a function of the particle diameter for both mechanical and combined mechanical-thermal couplings. The difference between the two cases is minimal, and Nu_h is very close to 0 despite the fact that the Reynolds number (Fig. 16) and the convective contribution (Fig. 17) increase for larger particles. The figures clearly show that this increase

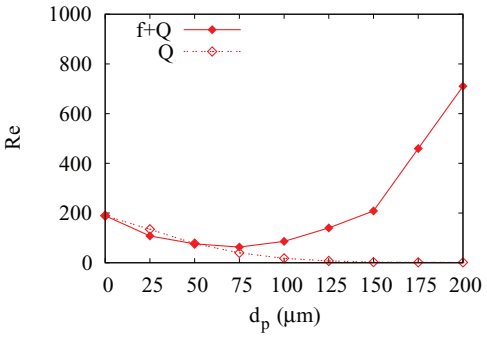

FIG. 16. (Color online) Fluid Reynolds number calculated with the volume- and time-averaged r.m.s. velocity as a function of the particle diameter d_p for "hot" particles, $T_p = T_h$. The dashed line (label Q) shows results with thermal coupling only, and the solid line (labeled $f + Q$) results with combined thermal and mechanical coupling.

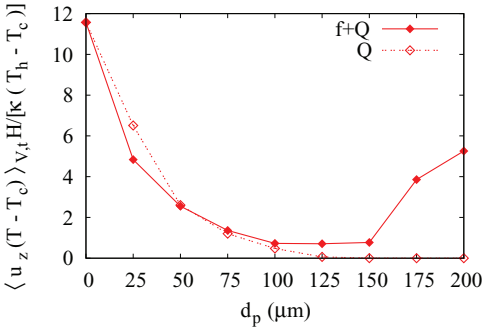

FIG. 17. (Color online) Convective contribution to the hot-plate Nusselt number, Eq. (20), as a function of the particle diameter d_p for "hot" particles, $T_p = T_h$. The dashed line (labeled Q) shows results with thermal coupling only, and the solid line (labeled $f + Q$) results with combined thermal and mechanical coupling.

is a purely mechanical effect that has no bearing on the heat transfer.

VI. SUMMARY AND CONCLUSIONS

We have studied the effect of particles with a prescribed temperature falling under gravity in a Rayleigh-Bénard cell filled with a much lighter fluid (gas). We have considered different particle diameters and cases in which the particle temperature equals either one of the prescribed temperatures at the hot or cold bases of the cell or their average. We have also investigated the separate effects of purely mechanical, purely thermal, and combined mechanical and thermal couplings between the particles and the fluid. We have found a very strong effect of the mechanical coupling with increasing particle diameter: the falling particles tend to drag fluid down, which constrains the ascending stream to a smaller and smaller fraction of the cross section, thus increasing its velocity.

A rather unexpected result has been a very unusual kind of reverse "one-way coupling" between the particles and the fluid, in the sense that the results show a very small effect of the fluid on the particles but a large effect of the particles on the fluid, despite the smallness of the Stokes numbers. This result is the consequence of the very strong constraint on the fluid behavior that is imposed by the vanishing of the fluid vertical velocity averaged over the cross section of the cell. The fact that similar features are found also for warm and hot particles suggests that it is a robust outcome of the physics of the process investigated that would persist even if the particles were allowed to change their temperature in response to heat exchange with the fluid.

ACKNOWLEDGMENTS

The authors are grateful to Professors D. Lohse and R. Verzicco for several useful suggestions. We acknowledge the kind support provided by the IT staff at the Centro Cultura Innovativa d'Impresa, University of Salento, where the computations where carried out. P.O. and A.P. gratefully acknowledge support by FIRB under Grant No. RBFR08QIP5_001 and NSF under Grant No. CBET 1258398, respectively.

[1] E. Bodenschatz, W. Pesch, and G. Ahlers, Annu. Rev. Fluid Mech. **32**, 709 (2000).
[2] G. Ahlers, S. Grossmann, and D. Lohse, Rev. Mod. Phys. **81**, 503 (2009).
[3] D. Lohse and K.-Q. Xia, Annu. Rev. Fluid Mech. **42**, 335 (2010).
[4] R. A. Shaw, Annu. Rev. Fluid Mech. **35**, 183 (2003).
[5] A. M. Jellinek and R. C. Kerr, J. Volcanol. Geotherm. Res. **110**, 253 (2001).
[6] I. Molina, A. Burgisser, and C. Oppenheimer, J. Geophys. Res. Solid Earth **117**, B07209 (2012).
[7] V. K. Dhir, Annu. Rev. Fluid Mech. **30**, 365 (1998).
[8] J.-K. Kim and R. Smith, Chem. Eng. Sci. **56**, 3641 (2001).
[9] J. Q. Zhong, D. Funfschilling, and G. Ahlers, Phys. Rev. Lett. **102**, 124501 (2009).
[10] D. S. Wen and Y. L. Ding, IEEE Trans. Nanotech. **5**, 220 (2006).
[11] J. Schumacher and O. Pauluis, J. Fluid Mech. **648**, 509 (2010).
[12] T. Weidauer, O. Pauluis, and J. Schumacher, Phys. Rev. E **84**, 046303 (2011).
[13] P. Oresta, R. Verzicco, D. Lohse, and A. Prosperetti, Phys. Rev. E **80**, 026304 (2009).
[14] L. E. Schmidt *et al.*, New J. Phys. **13**, 025002 (2011).
[15] R. Lakkaraju *et al.*, Phys. Rev. E **84**, 036312 (2011).
[16] R. Lakkaraju *et al.*, Proc. Natl. Acad. Sci. USA **23**, 110 (2013).
[17] E. Climent and J. Magnaudet, Phys. Fluids **18**, 103304 (2006).
[18] I. M. Mazzitelli and D. Lohse, Phys. Rev. E **79**, 066317 (2009).
[19] B. Shotorban, F. Mashayek, and R. V. R. Pandya, Int. J. Multiphase Flow **29**, 1333 (2003).
[20] F. Zonta, C. Marchioli, and A. Soldati, Acta Mech. **218**, 357 (2011).
[21] B. Arcen, A. Taniere, and M. Khalij, Int. J. Heat Mass Transf. **55**, 6519 (2012).
[22] R. Puragliesi *et al.*, Int. J. Heat Fluid Flow **32**, 915 (2011).
[23] J. K. Eaton, Int. J. Multiphase Flow **35**, 792 (2009).
[24] S. Elghobashi, Appl. Sci. Res. **52**, 309 (1994).
[25] A. Ferrante and S. Elghobashi, Phys. Fluids **15**, 315 (2003).
[26] S. Balachandar and J. K. Eaton, Annu. Rev. Fluid Mech. **42**, 111 (2010).
[27] F. P. Incropera, D. P. DeWitt, T. L. Bergman, and A. S. Lavine, *Fundamentals of Heat and Mass Transfer*, 7th ed. (John Wiley & Sons, Hoboken, NJ, 2011).